Conceptual Design of a Dispersion Interferometer Using a Ratio of Modulation Amplitudes

Tsuyoshi AKIYAMA, Kazuo KAWAHATA, Shigeki OKAJIMA[1)] and Kazuya NAKAYAMA[1)]

National Institute for Fusion Science, 322-6 Oroshi-cho, Toki 509-5292, Japan

[1)]*Chubu University, 1200, Matsumoto-cho,Kasugai 487-8501, Japan*

(Received 5 January 2009 / Accepted 11 May 2009)

Since a dispersion interferometer is free from mechanical vibrations, it does not need a vibration compensation system even for a probe beam with a short wavelength. This paper describes a new signal processing of the dispersion interferometer using a ratio of modulation amplitudes with a photoelastic modulator. The proposed method is immune to changes in detected signal intensities, thus making the signal processing system simple. Designs of the optical system of the dispersion interferometer for proof of principle, especially specification of a nonlinear optical crystal, are also shown.

Keywords: interferometer, dispersion interferometer, non-linear crystal, photoelastic modulator, CO_2 laser

DOI: 10.1585/pfr.5.S1041

1. Introduction

High reliability and resolutions are required for electron density measurements in fusion devices in order to control plasmas and understand plasma physics.

Conventional heterodyne interferometry is widely used and has a high-density resolution. It, however, in a high-density range suffers from fringe jump errors, which degrade the interferometer's reliability. Recently, the Large Helical Device (LHD) developed a high-density operation regime whose central electron density is up to several times 10^{20} m^{-3} [1], and the expected density range in ITER is about 1×10^{20} m^{-3} [2]. Consequently, the problem of fringe jump is becoming more significant. While a short-wavelength laser can reduce probabilities of fringe jumps, phase errors caused by mechanical vibrations become significant. They have to be suppressed with a vibration isolator or be compensated for by adopting two-color interferometry, which consists of two probe beams (light sources) with different wavelengths. Even then, it is difficult to eliminate the vibration components completely because of slight differences in the optical path and wavefronts of the probe beams. Besides, an optical system becomes complex and expensive.

One candidate for a solution is a density measurement with a polarimeter based on the Faraday effect [3–5] or the Cotton–Mouton effect [6–8]. Although density resolutions of polarimeters are less than those of interferometers, polarimeters do not suffer from fringe jump errors and are in principle immune to mechanical vibrations.

Another candidate for a solution is a dispersion interferometer [9]. It is also insensitive to mechanical vibrations, and hence does not need the vibration isolator and the two-color interferometry system even if a short-wavelength laser, a CO_2 laser or a Nd:YAG laser, is used.

This paper describes a new signal processing of the dispersion interferometer using a ratio of modulation amplitudes. The proposed method simplifies the signal processing and can remove measurement errors due to changes in the detected signal intensity. Section 2 briefly explains the principle of the dispersion interferometer and the new proposed signal processing. Section 3 shows a design of the proposed dispersion interferometer for the proof of the principle. Section 4 contains a summary.

2. Principle of a Dispersion Interferometer

Dispersion interferometers were proposed in the early 1980s [10, 11] and were used for density measurements of laser-produced plasmas, contouring the surface of three-dimensional objects and so on. Physical quantities to be measured were evaluated from the interferogram. In the 1990s, dispersion interferometers were adopted for measurements of the line averaged electron density of fusion plasmas (the mirror device: the gas-dynamic trap device) [9]. As described in Sec. 2.1, the density was obtained from the phase shift of the interference signal, which was almost the same as that of a homodyne interferometer. Later, the phase modulation technique [12] was introduced to the dispersion interferometer on TEXTOR in order to overcome the disadvantages of homodyne detection as shown in Sec. 2.2. The new signal processing method proposed in this paper is shown in Sec. 2.3. It is a simple technique to improve phase resolution for the above dispersion interferometer with a phase modulation.

author's e-mail: takiyama@lhd.nifs.ac.jp

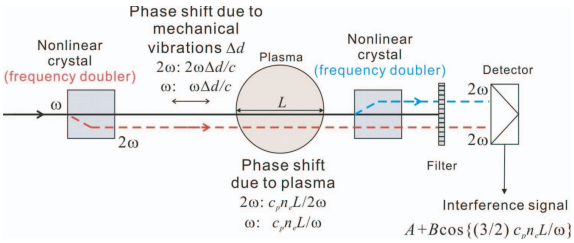

Fig. 1 Basic dispersion interferometer.

2.1 Basic dispersion interferometer

Figure 1 demonstrates the principle of the basic dispersion interferometer [9]. A probe beam with an angular frequency ω passes through a type-I nonlinear crystal to generate the second harmonic with a polarization angle perpendicular to that of the fundamental. The fundamental and the second harmonic components propagate along almost the same optical path. Phase shifts due to changes in the optical path length Δd by mechanical vibrations are $\omega\Delta d/c$ and $2\omega\Delta d/c$, respectively. The phase shifts due to a plasma are $c_p\bar{n}_eL/\omega$ and $c_p\bar{n}_eL/(2\omega)$, where $c_p = e^2/(2\varepsilon_0 m_e c)$, $\bar{n}_e$ is the line averaged electron density, and L is the optical path length in the plasma. After passing through the plasma, the second harmonic is generated from the fundamental again with the other nonlinear crystal. The remaining fundamental, which is not converted into the second harmonic, is cut by a following filter and only the second harmonics go into the detector. Phases of these second harmonics φ_1 and φ_2 (second harmonics which are generated by the first and the second nonlinear crystals are noted as 1 and 2, respectively) are given as follows:

$$\begin{aligned}\varphi_1 &= 2(\omega t + \omega\Delta d/c + c_p\bar{n}_eL/\omega + \phi_1),\\ \varphi_2 &= 2\omega t + 2\omega\Delta d/c + c_p\bar{n}_eL/(2\omega) + \phi_2,\end{aligned} \tag{1}$$

where ϕ_1 and ϕ_2 are initial phases of second harmonics. The detected interference signal I between these second harmonic components becomes

$$\begin{aligned}I &= A + B\cos(\varphi_1 - \varphi_2) = A + B\cos\left(\frac{3}{2}\frac{c_p\bar{n}_eL}{\omega} + \phi\right),\\ A &= I_1 + I_2,\ B = 2\sqrt{I_1I_2}\,,\end{aligned} \tag{2}$$

I_1, I_2: intensities of second harmonics, $\phi = 2\phi_1 - \phi_2$.

As shown in Eq. (2), the phase shift due to vibrations is canceled out automatically. Therefore, the phase of the interference signal is determined by only the dispersion of the plasma and is free from vibrations even with short-wavelength lasers.

2.2 Dispersion interferometer with a phase modulation

As Eq. (2) is almost the same as the interference signal of a homodyne interferometer, the basic dispersion interferometer has the same disadvantages as the homodyne ones: (i) restriction of phase where Eq. (2) is a monotonic function and (ii) the necessity for calibration experiments of the detected intensity A and B and their variations during discharges lead to phase errors. The phase modulation method [12] with an electro-optical modulator (EOM) can reduce the influence of the intensity variations. The EOM, operating with a drive signal of $\pi\sin\Omega t$, is inserted between the first nonlinear crystal and the plasma. It gives a phase modulation of $\pi\sin\Omega t$ only for the second harmonics. As a result, the detected modulated interference signal I_{pm} can be given by

$$I_{pm} = A + B\cos\left(\pi\sin\Omega t + \frac{3}{2}\frac{c_p\bar{n}_eL}{\omega} + \phi\right). \tag{3}$$

I_{pm} is directly digitized with a higher sampling frequency than Ω. Because of phase modulation, the amplitude of I_{pm} changes between the maximum $(A + B)$ and the minimum $(A - B)$. A and B are assumed to be constant during one modulation period and are evaluated from the digitized signal. Then A is subtracted from the digitized signal and the amplitude of I_{pm} is normalized by B. The drive signal of the EOM is also digitized coincidently, and the times t_0 when $\sin\Omega t_0 = 0$ are determined. At t_0, the normalized signal I_{pm}^{norm} is given by

$$I_{pm}^{norm} = \cos\left(\frac{3}{2}\frac{c_p\bar{n}_eL}{\omega} + \phi\right). \tag{4}$$

$\bar{n}_e$ can be calculated from the arccosine of Eq. (4).

2.3 Dispersion interferometer using a ratio of modulation amplitudes

Figure 2 shows a schematic view. A photoelastic modulator (PEM) with a stable modulation frequency is adopted for the phase modulation instead of the EOM. The modulator axis of the PEM is arranged parallel to the polarization direction of the fundamental to give phase modulations to only the fundamental. In this configuration, an interference signal $I(t)$, almost the same as Eq. (3), is given by,

$$\begin{aligned}I(t) &= A + B\cos\left(2\rho_0\sin\omega_{\rm m}t + \frac{3}{2}\frac{c_p\bar{n}_eL}{\omega} + \phi\right)\\ &= A + B\left\{\cos(2\rho_0\sin\omega_{\rm m}t)\cos\left(\frac{3}{2}\frac{c_p\bar{n}_eL}{\omega} + \phi\right)\right\}\\ &\quad - B\left\{\sin(2\rho_0\sin\omega_{\rm m}t)\sin\left(\frac{3}{2}\frac{c_p\bar{n}_eL}{\omega} + \phi\right)\right\},\end{aligned} \tag{5}$$

where ρ_0 is the maximum retardation of the PEM, determined by the voltage applied to the PEM, and $\omega_{\rm m}$ is the modulation frequency of the PEM. Here, $\cos(2\rho_0\sin\omega_{\rm m}t)$ and $\sin(2\rho_0\sin\omega_{\rm m}t)$ can be expanded with the Bessel function of order of n $J_{\rm n}$.

$$\begin{aligned}\cos(2\rho_0\sin\omega_{\rm m}t) &= J_0(2\rho_0) + 2\sum_{n=1}^{\infty}J_{2n}(2\rho_0)\cos(2n\omega_{\rm m}t),\\ \sin(2\rho_0\sin\omega_{\rm m}t) &= 2\sum_{n=1}^{\infty}J_{2n-1}(2\rho_0)\sin\{(2n-1)\omega_{\rm m}t\}.\end{aligned} \tag{6}$$

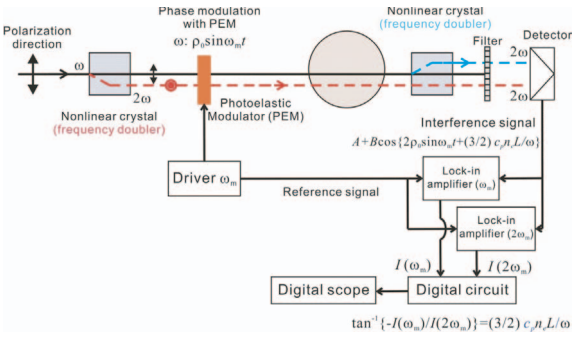

Fig. 2 Dispersion interferometer with a photoelastic modulator (PEM) and signal processing using a ratio of modulation amplitudes.

In this way, the detected interference signal $I(t)$ can be expanded with harmonics of $\omega_{\rm m}$. The following amplitudes of fundamental and second harmonics $I_{\omega_{\rm m}}$ and $I_{2\omega_{\rm m}}$ of the modulation frequency $\omega_{\rm m}$ can be measured with lock-in amplifiers.

$$I_{\omega_{\rm m}} = -2BJ_1(2\rho_0)\sin\left(\frac{3}{2}\frac{c_p\bar{n}_eL}{\omega}+\phi\right),$$
$$I_{2\omega_{\rm m}} = 2BJ_2(2\rho_0)\cos\left(\frac{3}{2}\frac{c_p\bar{n}_eL}{\omega}+\phi\right). \quad (7)$$

From the ratio of these amplitudes, $\bar{n}_e$ can be obtained.

$$\bar{n}_e = \frac{2}{3}\frac{\omega}{c_pL}\left\{\tan^{-1}\left(\frac{I_{\omega_{\rm m}}}{I_{2\omega_{\rm m}}}\right)-\phi\right\}. \quad (8)$$

Here, ρ_0 is set at 1.3 radians by applying adequate voltage to the photoelastic material for $J_1(2\rho_0) = J_2(2\rho_0)$. Since tangent diverges at $\pm\pi/2$, if necessary, the initial phase may be adjusted by inserting a phase object after the filter.

An ellipsometer similarly uses sinusoidal phase modulation and harmonics for accurate measurement of the polarization state. This new method of phase extraction is completely free from variations of detected intensities A and B. In addition, the processing is simple and suited to real time measurements.

3. Conceptual Design of a Dispersion Interferometer Using the Ratio of Modulation Amplitude

To prove the principle, we are designing a dispersion interferometer with a CO_2 laser whose wavelength is 10.6 μm. The dispersion interferometer on TEXTOR also uses the CO_2 laser [12]. The CO_2 laser to be used is a GN-802-GES (MPB Technology Inc.) with an output power of 7.5 W or an LC-25 (DEOS) with 25 W. Either one of them will be selected depending on its signal-to-noise ratio (SNR). An important component for a good SNR is a nonlinear crystal for second-harmonic generation (SHG), because the power of the second harmonics depends strongly on the specifications of the nonlinear crystal.

Table 1 Parameters of $AgGaSe_2$ for 10.6 μm.

Transparency (μm)	0.8-18
Refractive index n_o (10.6 μm)	2.5912
Refractive index n_e (10.6 μm)	2.5579
Refractive index n_o (5.3 μm)	2.1634
Refractive index n_e (5.3 μm)	2.5808
$d_{\rm eff}$ (definition: $P = dE^2$)	2.47×10^{-22}
Surface damage threshold $P_{\rm sd}$ (kW/cm^2, CW)	33-45
Thermal-lensing threshold $P_{\rm l}$ (kW/cm^2)	2
Thermal conductivity (W/cm/K)	0.011

3.1 Design of a nonlinear crystal for SHG

Silver gallium selenide ($AgGaSe_2$) is commonly used for SHG of 10.6 μm laser light. Table 1 [13–15] summarizes its properties. The conversion efficiency $\eta = P_{2\omega}/P_\omega$, where $P_{2\omega}$ and P_ω are the powers of the second harmonic and the fundamental, respectively, is given by [15]

$$\eta = 2\left(\frac{\mu}{\varepsilon_0}\right)^{3/2}\frac{\omega^2d_{\rm eff}^2l^2}{n^3}\left(\frac{P_\omega}{\pi w_0^2}\right)\left\{\frac{\sin(\Delta kl/2)}{\Delta kl/2}\right\}^2, \quad (9)$$
$$\Delta k \equiv k_{2\omega}-2k_\omega,$$

where $d_{\rm eff}$ is the effective nonlinearity, l is the length of the crystal, n is the refractive index of the fundamental, w_0 is the beam waist ($1/e^2$ power radius), and $k_{2\omega}$ and k_ω are wavenumbers of the second harmonics and the fundamental, respectively. The last term that includes Δk stands for the phase matching condition. As mentioned in Sec. 3.2, that condition is determined by the angle between the beam path and the optic axis of the crystal. Here, the phase matching condition is assumed to be satisfied; the term is unity. It is noted that Eq. (9) presumes a plane wave for incident light. This is approximately valid when the length of the crystal is less than the confocal focusing length $z_0 = \pi w_0^2 n/\lambda$ of the Gaussian beam.

In general, η for continuous-wave (cw) laser light is small (on the order of 0.1%). To improve the SNR, it is favorable to increase the power of the second harmonic as much as possible. Eq. (9) indicates that η increases with the power density of the incident beam. On the other hand, there are some limitations in the power density and the crystal length as follows.

The maximum power density $P_0 = 2P_{\rm total}/(\pi w_0^2)$ of the focused Gaussian beam into the nonlinear crystal should be smaller than the surface damage threshold $P_{\rm sd}$ of 33 kW/cm^2 for a cw laser. Here, $P_{\rm total}$ is the total incident power. In the case of $AgGaSe_2$, the thermal-lensing effect, which decreases the SHG efficiency, should be considered because of the small thermal conductivity of $AgGaSe_2$. A threshold $P_{\rm l}$ for the thermal-lensing effect of 2 kW/cm^2 is reported in Ref. 13 and is smaller than $P_{\rm sd}$. Thus, allowable beam waist is determined by $P_{\rm l}$. In this design, the

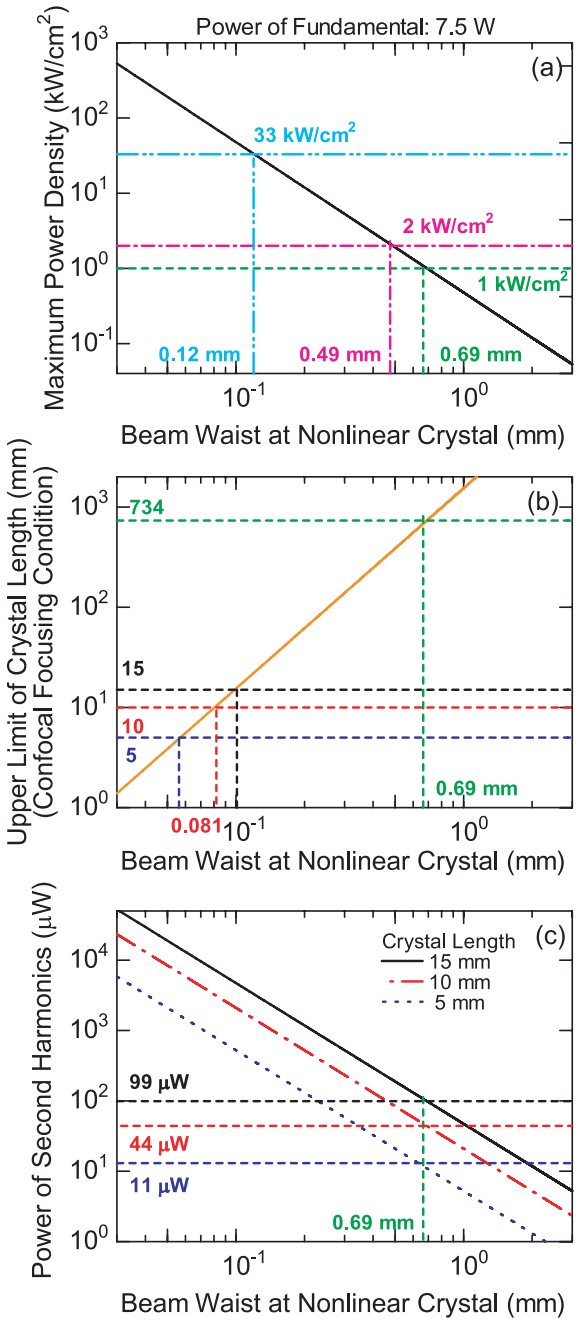

Fig. 3 Dependence of (a) maximum power density, (b) upper limit of crystal length, and (c) power of second harmonic component on a beam waist at a nonlinear crystal in the case of an incident beam with a power of 7.5 W. The nonlinear crystal is $AgGaSe_2$.

maximum power density is set at half of P_1, 1 kW/cm^2, for safety. The resultant beam waist is 0.69 mm, as shown in Fig. 3 (a), for a total incident power of 7.5 W.

The commercially available length of the $AgGaSe_2$ crystal is less than about 20 mm at present. The upper limit of the crystal length, determined by the confocal focusing length, is much larger than the available length for a beam waist of 0.69 mm, as shown in Fig. 3 (b).

Figure 3 (c) shows the power of the generated second harmonic calculated with Eq. (9). In the case of a 15 mm-long crystal, 99 μW is generated from an incident beam with a power of 7.5 W and beam waist of 0.69 mm. The transmissivity at the second harmonic of zinc selenide (ZnSe) with anti-reflection coating at the fundamental, which is used for the PEM and two vacuum windows (not shown in Fig. 2), is about 0.65. The transmissivity of an IR filter made of sapphire that eliminates the fundamental (see Fig. 2) is about 0.7. As a result, the total transmissivity of the second harmonics that are generated in the first nonlinear crystal is $0.65^3 \times 0.7 = 0.19$. When the thermoelectrically cooled IR photovoltaic detector PVI-3TE-5 (Vigo system, responsivity = 2 (A/W)) and the preamplifier STCC-04 (Vigo system, transimpedance = 10^5 (V/A)) are used, the output voltages I_1 and I_2 become as follows.

$$I_1 = (99 \times 10^{-6}) \times 0.19 \times 2 \times 10^5 = 3.8\text{V},$$

$$I_2 = (99 \times 10^{-6}) \times 0.7 \times 2 \times 10^5 = 14\text{V}.$$

Considering the efficiency of interference, the reflectivity of mirrors, and so on, the detected power will be slightly smaller. Nevertheless, these generated powers of the second harmonics are enough to be detected.

3.2 Phase matching condition

The second harmonic is continuously generated along the optical path in the nonlinear crystal. If phases of the second harmonics which are generated at the entrance and the central region in the crystal are different, they interfere with each other and the total power of the second harmonic decreases. In order to suppress that interference, the phase of the second harmonic should be matched (phase matching condition). For that purpose, the fundamental is injected into the crystal at a certain angle θ_m against the optic axis of the crystal to satisfy $n_e^{(2\omega)} = n_o^{(\omega)}$ based on the birefringence. In the case of the type-I nonlinear crystal, the fundamental and the second harmonic are ordinary and extraordinary waves, respectively. θ_m is given by following expression [15].

$$\sin^2\theta_m = \frac{\left\{n_o^{(\omega)}\right\}^{-2} - \left\{n_o^{(2\omega)}\right\}^{-2}}{\left\{n_e^{(2\omega)}\right\}^{-2} - \left\{n_o^{(2\omega)}\right\}^{-2}}. \tag{10}$$

Assigning refractive indexes, θ_m of $AgGaSe_2$ becomes 55.4 deg. Δk is also given by

$$\Delta kl/2 \approx -\frac{\omega l}{c}\sin(2\theta_m)\frac{\left\{n_e^{(2\omega)}\right\}^{-2} - \left\{n_o^{(2\omega)}\right\}^{-2}}{2\left\{n_o^{(\omega)}\right\}^{-3}}(\theta-\theta_m), \tag{11}$$

and $F = \{\sin(\Delta kl/2)/(\Delta kl/2)\}^2$ is plotted in Fig. 4. The half width of F for the 15-mm long crystal is only 0.3 deg.

Deviation from the phase matching angle may occur because of beam bending due to an electron density gradient. Deviation is estimated to be negligible, on the order

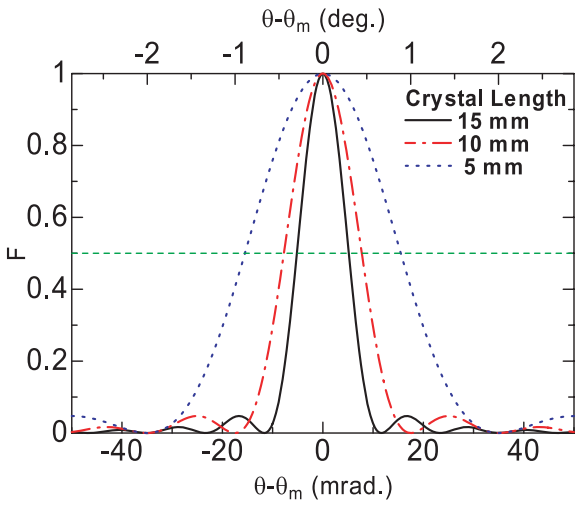

Fig. 4 Phase matching condition for $AgGaSe_2$.

of 0.01 deg., in the case of a LHD plasma with a density profile of $1 \times 10^{20}(1-\rho^8)\,\mathrm{m}^{-3}$. However, it may become significant to the reduction of the SHG in higher-density range, where the beam bending angle becomes larger.

3.3 Potential problems

Because the power of the second harmonic is proportional to P_ω^2, beam dividing for multi-channel measurement strongly affects the SHG at the second nonlinear crystal. The possible number of channels will be determined by the laser power, efficiency of SHG, sensitivity of the detector, and so on.

Displacement of the fundamental and the second harmonic beams decreases interference and the accuracy of vibration-cancelation. The displacement is caused by effects of walk-off in the nonlinear crystal and differences in the beam refraction in plasmas. In our system, beam displacements are estimated to be less than about 0.2 mm, much smaller than an expected beam radius of about 10 mm for either effect. However, displacement may become significant in the case of a long beam transmission or a large wedge angle of vacuum windows.

4. Summary

A dispersion interferometer is a candidate for reliable electron density measurement. We propose the dispersion interferometer using a ratio of modulation amplitudes with a PEM. This method removes measurement errors due to changes in the detected signal intensity and makes the signal processing simple and easily applicable in real time feedback control. $AgGaSe_2$ is selected for SHG of CO_2 laser light. The power of the second harmonics is estimated for proof of the principle experiments.

Acknowledgements

This work was supported by Grant-in-Aid for Young Scientists (B) (20760584) and partly by Grant-in-Aid for Scientific Research on Priority Areas “Advanced Diagnostics for Burning Plasmas” (16082208).

[1] N. Ohyabu, T. Morisaki, S. Masuzaki, R. Sakamoto, M. Kobayashi, J. Miyazawa, M. Shoji, A. Komori, O. Motojimi and LHD Experimental Group, Phys. Rev. Lett. **97**, 055002 (2006).
[2] Y. Shimomura, R. Aymar, V.A. Chuyanov, M. Huguet, H. Matsumoto, T. Mizoguchi, Y. Murakami, A.R. Polevoi and M. Shimada, Nucl. Fusion **41**, 309 (2001).
[3] Y. Kawano, S. Chiba and A. Inoue, Rev. Sci. Instrum. **72**, 1068 (2001).
[4] T. Akiyama, K. Kawahata, Y. Ito, S. Okajima, K. Nakayama, S. Okamura, K. Matsuoka, M. Isobe, S. Nishimura, C. Suzuki *et al.*, Rev. Sci. Instrum. **77**, 10F118 (2006).
[5] M. A. Van Zeeland, R. L. Boivin, T. N. Carlstrom and T. M. Deterly, Rev. Sci. Instrum. **79**, 10E719 (2008).
[6] Ch. Fuchs and H. J. Hartfuss, Phys. Rev. Lett. **81**, 1626 (1998).
[7] T. Akiyama, K. Kawahata, Y. Ito, S. Okajima, K. Nakayama, S. Okamura, K. Matsuoka, M. Isobe, S. Nishimura, C. Suzuki *et al.*, Rev. Sci. Instrum. **77**, 10F118 (2006).
[8] A. Boboc, L. Zabeo and A. Murari, Rev. Sci. Instrum. **77**, 10F324 (2006).
[9] V. P. Drachev, Yu. I. Krasnikov and P. A. Bagryansky, Rev. Sci. Instrum. **64**, 1010 (1993).
[10] F. A. Hopf, A. Tomita and G. Al-Jumaily, Optics letters **5**, 386 (1980).
[11] Kh. P. Alum, Yu. V. Koval’chuk and G. V. Ostrovskaya, Sov. Tech. Phys. Lett. **7**, 581 (1981).
[12] P. A. Bagryansky, A. D. Khilchenko, A. N. Kvashnin *et al.*, Rev. Sci. Instrum. **77**, 053501 (2006).
[13] S. Ya Tochitsky, V. O. Petukhov, V. A. Gorobets, V. V. Chuakov and V. N. Jakimovich, Appl. Optics **36**, 1882 (1997).
[14] Cleverland Crystals Inc.
[15] A. Yariv, “Optical Electronics in Modern Communications fifth edition”, Oxford University Press.